DAMAGE ASSESSMENT OF BUILDINGS IN KATHMANDU DUE TO THE 2015 NEPAL EARTHQUAKE USING TERRASAR-X IMAGERY

Rendy Bahri[1], Wen Liu [2] and Fumio Yamazaki[3]

Department of Urban Environment Systems, Chiba University
1-33 Yayoi-cho, Inage-ku, Chiba 263-8522, Japan;
[1] rendy.bahri@gmail.com; [2] wen.liu@chiba-u.jp; [3] fumio.yamazaki@faculty.chiba-u.jp

KEY WORDS: TerraSAR-X, building damage assessment, rapid damage mapping, 2015 Gorkha earthquake

ABSTRACT: Damage assessment is an important issue for emergency response and recovery activities after the occurrence of nature disasters. In this regard, satellite remote sensing is recognized as an effective tool for detecting and monitoring affected areas. Since SAR sensors can capture images not only at daytime but also at nighttime and under cloud-cover conditions, we used multi-temporal high-resolution TerraSAR-X images to detect the changes of urban areas in Kathmandu, the capital city of Nepal, which was severely affected by the 2015 Gorkha earthquake on April 25, 2015 with Mw 7.8. It caused the collapse of many buildings including those in Kathmandu Durbar Square. TerraSAR-X images obtained before and after the earthquake were utilized for calculating the difference and correlation coefficient of the SAR backscatter, within the layover area of a large building in order to extract severely damaged buildings in the central Kathmandu. The affected areas were identified by high values of the difference and low values of the correlation coefficient. The pre- and post-event high-resolution optical satellite images were employed as ground truth data to verify our results. As the result, the both indices were found to be suitable for identifying severely affected buildings. Hence we used them to create a rapid preliminary damage map that can be used in emergency response.

1. INTRODUCTION

The 2015 Gorkha, Nepal, earthquake with Mw 7.8 occurred at 11:56 (the local time) on 25 April and killed more than 8,800 people and injured more than 23,000 people. Its epicenter was in the east of Lamjung District, which is 80-km northwest of the capital city, Kathmandu. The focal depth was apprixamately15 km. A major aftershock of Mw 6.7 occurred on 26 April 2015, in the same region at 12:55 NST, with the epicenter was located at about 17-km south of Kodari in Sindhupalchowk District. Kathmandu is one of the severe affected cities due to the earthquake. Centuries-old buildings were destroyed at UNESCO World Heritage sites in the Kathmandu Valley, including some at the Kathmandu, Patan, and Bhaktapur Durbar Squares, the Changu Narayan Temple, and the Swayambhunath Stupa. Kathmandu City is characterized by its high population density and vast manmade features in comparison to the surrounding areas. It means this urban area is the very important function place for the country. Hence it is very important to grasp the situation of the affected areas in the aftermath of the earthquake to take some proper actions.

Remote sensing is recognized as an effective tool for detecting and monitoring the affected areas after the occurrence of a natural disaster. Based on the sensor types, there are mainly two categories of remote sensing: passive remote sensing (mainly optical sensors) and active remote sensing (mainly radar sensors). Optical satellite systems only work in the daytime and cannot observe objects under cloud-cover conditions. However, radar systems as Synthetic Aperture Radar (SAR) overcome this problem. Hence they are widely used in various emergency situations. SAR images have also been used in interferometric analysis to investigate damage to buildings (Ito et al., 2000; Yonezawa and Takeuchi, 2001). Comparing the changes in pre- and post-event SAR intensity images, damage detection of buildings has been conducted by several researchers (Matsuoka and Yamazaki, 2004; Dell'Acqua and Gamba, 2012.). Recently, several studies attempted to detect damages caused by earthquakes at the scale of a single building unit, using both high-resolution optical and SAR images (Brunner et al., 2010; Uprety and Yamazaki, 2012; Miura et al., 2016) and by tsunami (Liu et al., 2013)

In this study, TerraSAR-X images obtained before and after the earthquake are used to detect the affected areas in Kathmandu to provide supportive information for emergency response. The difference and correlation coefficient of backscatter for each building are calculated in order to extract damaged buildings. The both indices are used to create a rapid damage map for emergency response activities. The pre- and post-event high-resolution optical satellite images are employed as ground truth data to verify our results.

2. THE STUDY AREA AND IMAGERY DATA USED

The study area is Kathmandu that is the capital city and the largest municipality in Nepal, as shown in **Figure 1(a)**, including the neighboring old capital city, Patan. This region is the only city in Nepal with the administrative status of Mahanagar (Metropolitan City), as compared to Upa-Mahanagar (Sub-Metropolitan City) or Nagar (City). Kathmandu is the core of Nepal's largest urban agglomeration, located in the Kathmandu Valley consisting of Lalitpur, Kirtipur, Madhyapur Thimi, Bhaktapur and a number of smaller communities.

The data employed in this research were taken by the TerraSAR-X (TSX) satellite system that launched on June 15, 2007 by the German Aerospace Center (DLR). TSX sensor acquires radar data in three main imaging modes, SpotLight (up to 1-m resolution), StripMap (up to 3-m), ScanSAR (up to 16-m). The pre-event image was captured on October 13, 2013 (18 months before the earthquake) and the post-event image was captured on April 27, 2015 (2 days after the earthquake). The acquisition mode of the both images was SpotLight (SL) with VV polarization with an incidences angle of 39.5 degrees at the center. These data were provided as the Single-look Slant-range Complex (SSC) products (PASCO, 2016). The satellite path was ascending with right-looking. The resolution was 1.6 m in the azimuth direction and 1.2 m in the slant-range direction.

The images were represented by the complex I and Q channels to preserve the amplitude and phase information. After several pre-processing steps using *ENVI/SARscape* software, these images were projected to a WGS84 reference ellipsoid with a pixel spacing of 1.25 m. Radiometric calibration was carried out by **Eqs. (1-3)** to get the backscattering coefficient (sigma naught, σ^0) in the ground range in the decibel (dB) unit.

$$\sigma^0(\mathrm{dB}) = \beta^0(\mathrm{dB}) + 10\log_{10}(\sin\theta_{loc}) \tag{1}$$

$$\beta^0 = 10\log_{10}(k_s \cdot DN^2) \tag{2}$$

$$\theta_{loc} = \frac{GIM - (GIM \bmod 10)}{100} \tag{3}$$

where σ^0 means the backscattering coefficient per unit area in the ground range, β^0 is the backscattering coefficient per unit area in the slant range; θ_{loc} is the incidence angle, k_s is the calibration factor; GIM means the Geo-coded incidence angle mask; DN is the digital number of the pixel.

After this conversion, an adaptive filter (Lee, 1980) was applied to the original SAR images to reduce the speckle noise, which makes the radiometric and textural aspects less efficient, and to improve the correlation coefficient between two images. In this study, we used the Lee filter with a 3×3 pixels window.

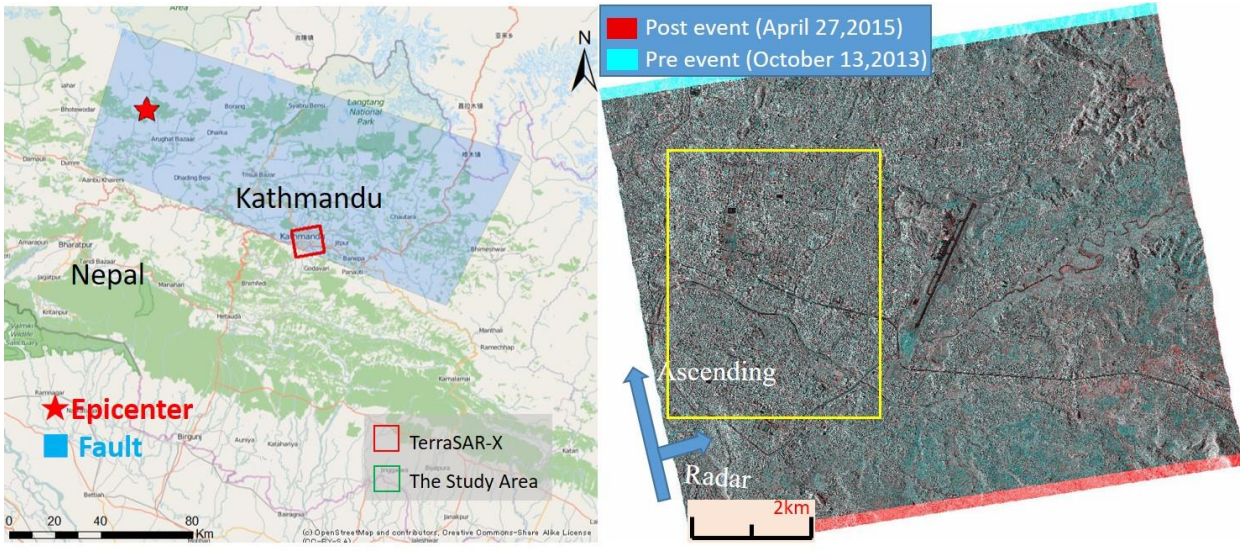

(a) Study area (b) Color composite VV polarizations

Figure 1. (a) Location of the study area in the central Nepal; (b) color composite of the pre- and post-event TSX images with VV polarizations, where the target area is shown in the yellow frame.

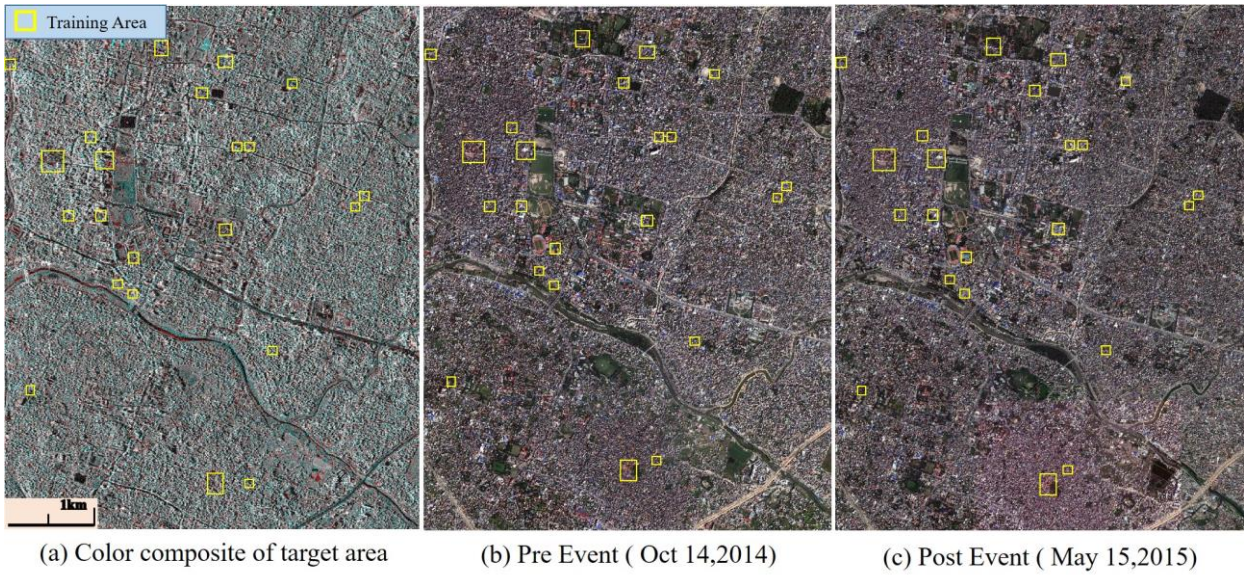

Figure 2. Close-up of the target area in the center of Kathmandu: (a) color composite of the pre- and post-event TSX images; (b) pre-event optical image taken on October 14, 2014 by WorldView-3; (c) post-event optical image taken on May 15, 2015 by Geoeye-1.

Figure 1(b) shows the color composite of the pre- and post-event TSX images with VV polarization. The target area at the center of Kathmandu was extracted and enlarged as shown in **Figure 2(a)**, including the Durbar Square, Tundikhel and Dharahara towers. Several changed areas could be confirmed by red (increased backscatter after the earthquake) and cyan (decreased backscatter after the earthquake) colors. The grey areas represent the unchanged areas over the time. Twenty-two (22) training areas shown by yellow polygons will be discussed later.

Pre-event and post-event high-resolution optical satellite images were also introduced as the truth data of building damage in the study area. The pre-event WorldView-3 (WV3) image was acquired on October 14, 2014 (04:59:37 UTC) with off-nadir angle 21° as shown in **Figure 2(b)**, and the post-event GeoEye-1 (GE1) image was acquired on May 15, 2015 (04:59:26 UTC) with off-nadir angle 23° as shown in **Figure 2(c)**. For the two temporal images, the bundle products of the panchromatic (Pan) and four multi-spectral (BGR and near-IR) bands were introduced. After a pansharpening process, the pre-event WV3 image has the spatial resolution of 31 cm and the post-event GE1 image was 50 cm.

3. DAMAGE DETECTION AND RESULTS

The change detection from the two-temporal SAR intensity images can be evaluated quantitatively by the difference of backscattering difference values (*d*) and the correlation coefficient *(r*), calculated by **Eqs. (4-5)**. Since the sizes of buildings in the target area were around 10 m - 15 m, a 11×11 pixels window (13.75 m×13.75 m) was adopted to obtain *d* and *r* in this study.

$$d = \bar{I}a_i - \bar{I}b_i \tag{4}$$

$$r = \frac{N\sum_{i=1}^{N} Ia_i Ib_i - \sum_{i=1}^{N} Ia_i \sum_{i=1}^{N} Ib_i}{\sqrt{(N\sum_{i=1}^{N} Ia_i^2 - (\sum_{i=1}^{N} Ia_i)^2)\cdot (N\sum_{i=1}^{N} Ib_i^2 - (\sum_{i=1}^{N} Ib_i)^2)}} \tag{5}$$

where Ia_i, Ib_i represent the *i*-th pixel values of the post- and pre-event SAR backscattering coefficient, respectively, and $\bar{I}a_i$ and $\bar{I}b_i$ are the average values of the 11×11 pixels surrounding the *i*-th pixel.

The correlation coefficient (*r*) is a scalar quantity between -1.0 and 1.0, and used to find the measure of correspondence between two-sample populations. A high positive value of *r* indicates no change between the pre- and post-event images whereas a low value indicates a strong possibility of change (Brown, 1992).

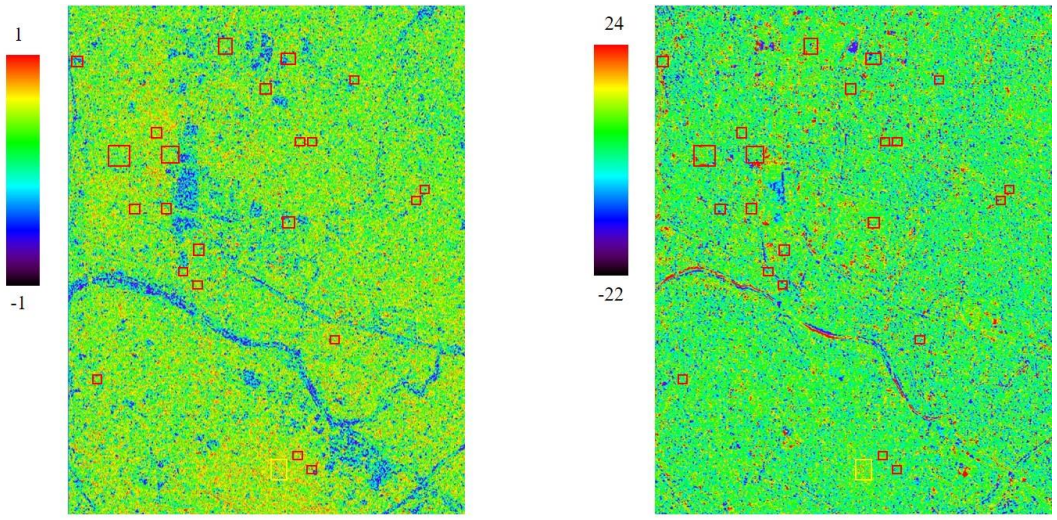

Figure 3. Correlation coefficient (*r*) and difference (*d*) of backscattering coefficient calculated from the pre- and post-event TSX images with a window size of 11×11 pixels, respectively.

Figure 3(a) shows the correlation coefficient (*r*), ranging from -1.0 to 1.0 and **Figure 3(b)** shows the difference of the backscattering coefficients (*d*) of the target area, ranging from -22 dB to 24 dB, between the pre- and the post-event images.

In this study, we selected 22 training areas including 41 collapsed/major damaged buildings (G4-G5 in the EMS-98 scale, abbreviated as "collapsed") and 50 no/minor damage buildings (G1-G3 in the EMS-98 scale, abbreviated as "survived") in the target area, to explain the tendency of the relationship between damaged and non-damaged areas in the backscattering difference and the correlation coefficient. These training areas are shown in **Figure 4**. Areas A-E and Kathmandu Durbar Square were used as the training areas in our previous study (Bahari et al., 2016). In the current study, in order to acquire highly credible results, we increased the number of collapsed buildings in the target area (area F-T and Patan Durbar Square) as shown **Figure 4**. The collapsed buildings are shown by red polygons and the survived buildings by green polygons. We selected them using the pre- and post-event optical images, field survey photos and aerial videos by drone. The break line shows the edge of the rooftop of a building, whereas the solid line shows the layover of a building's wall due to the oblique incidence of radar. The length of layover was calculated by **Eq. (6)**, in which H is a building height and θ is the SAR incidence angle.

$$L = \frac{H}{\tan\theta} \tag{6}$$

It was difficult to obtain the exact heights of buildings in Kathmandu, so in this study we selected tall and big buildings to recognize their heights easily. According to the optical images and filed survey photos, we divided the building heights into two types, a low building height as 10 m and a high building height as 15 m.

We calculated the average of correlation coefficient and the absolute difference of backscattering coefficients of the TSX images within the estimated layover area for each building, as shown in **Table 1**. The average of absolute difference for survived buildings was 0.67 dB with the standard deviation 0.52 dB, whereas the one for the collapsed buildings was 2.37 dB with standard deviation 1.78 dB. The collapsed buildings show high differences due to the change in the backscattering intensity. On the other hand, the average of correlation coefficient for 50 survived buildings was 0.42 with standard deviation 0.14. The high correlation value means the change before and after the earthquake was not significant. While the average of correlation coefficient for 41 collapsed buildings was 0.12 with standard deviation 0.19, which is quite low.

We can see the correlation coefficients for buildings Nos. 2, 4, 10, 16 are quite low compared with those of other survived buildings. As shown in **Figure 4,** these low values were caused by the rubbles of collapsed buildings and the change of vegetation. On the other hand, the correlation coefficients for buildings Nos. 127, 131, 137, 143, 146, 147, 148, and 150 are quite high, which are supposed to be low due to the changes caused by the earthquake.

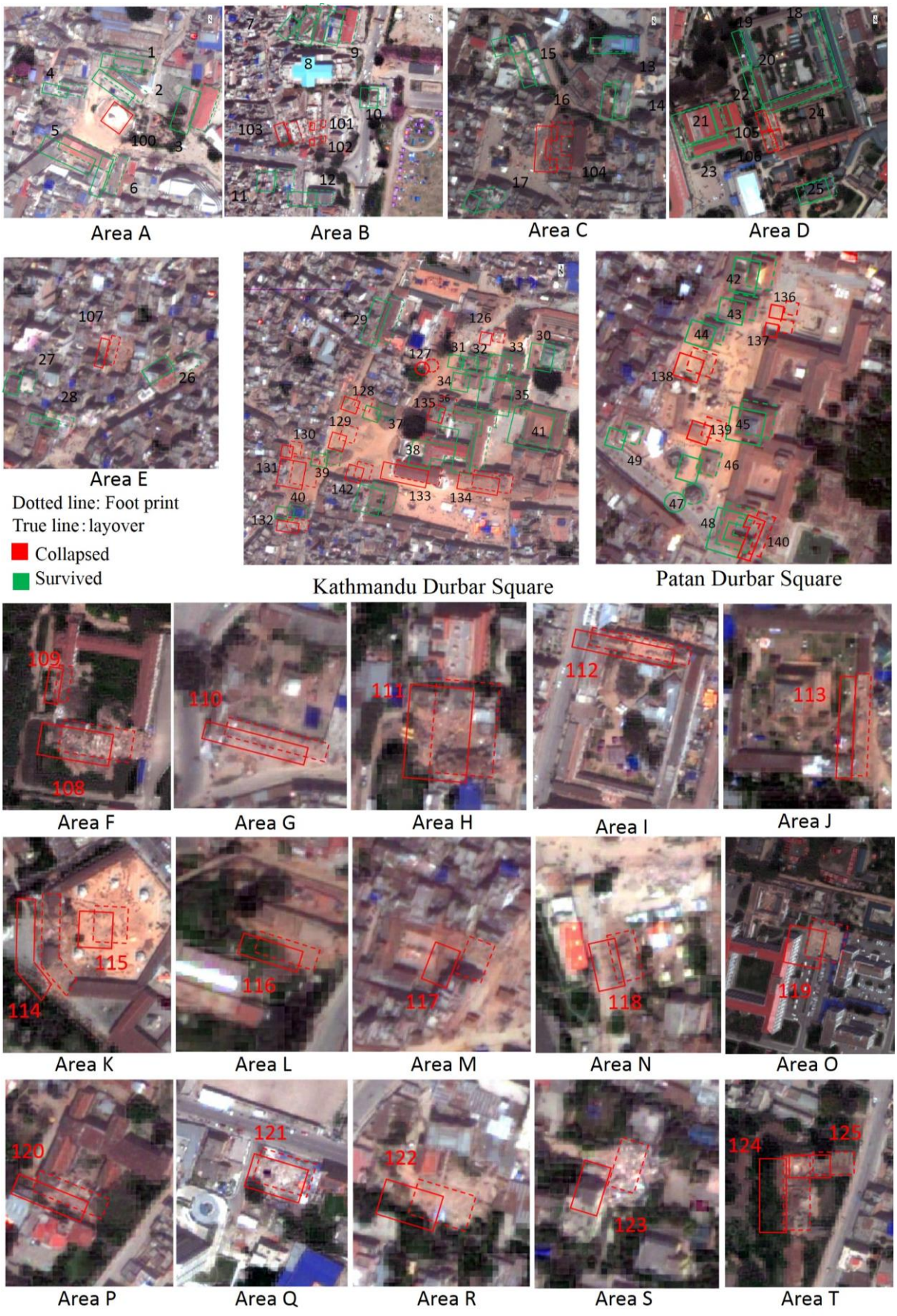

Figure 4. Training areas in the central Kathmandu: 41 collapsed or major damaged buildings and 50 non- or minor-damaged buildings with their roof-prints and layovers

Table 1. Correlation coefficient and absolute difference of backscattering coefficient inside the layover of each building

No・Minor damage building			Bldg No.	d [dB]	r
Bldg No.	d [dB]	r	26	0.20	0.43
1	0.59	0.32	27	0.70	0.46
2	0.88	0.21	28	0.28	0.43
3	0.14	0.35	29	1.02	0.32
4	0.40	0.20	30	0.96	0.48
5	0.60	0.47	31	1.20	0.43
6	0.76	0.33	32	1.05	0.66
7	0.39	0.49	33	1.24	0.28
8	0.31	0.52	34	2.00	0.37
9	1.18	0.32	35	0.21	0.49
10	0.79	0.22	36	0.33	0.39
11	0.41	0.52	37	1.94	0.44
12	0.80	0.53	38	1.47	0.41
13	0.99	0.28	39	0.67	0.37
14	0.50	0.34	40	0.28	0.66
15	1.87	0.41	41	0.54	0.49
16	0.46	0.19	42	1.61	0.45
17	0.88	0.49	43	0.12	0.72
18	0.95	0.27	44	0.00	0.69
19	0.00	0.34	45	1.32	0.46
20	0.40	0.38	46	0.10	0.45
21	0.57	0.50	47	0.14	0.57
22	0.20	0.28	48	0.10	0.44
23	0.60	0.41	49	0.11	0.84
24	0.00	0.31	50	1.02	0.27
25	0.40	0.43	Average	0.67	0.42
			Std Deviation	0.52	0.14

Collapsed・Major damage building			Bldg No.	d [dB]	r
Bldg No.	d [dB]	r	131	0.37	0.41
110	1.63	0.12	132	1.56	−0.03
111	5.47	−0.31	133	2.27	0.16
112	5.00	−0.27	134	1.89	−0.06
113	6.84	0.15	135	1.89	0.32
114	4.10	0.15	136	1.84	0.18
115	1.58	0.16	137	1.46	0.62
116	2.82	−0.11	138	5.48	0.25
117	5.23	−0.10	139	1.41	0.35
118	2.31	0.26	140	3.71	0.23
119	7.95	−0.02	141	3.40	0.24
120	0.61	0.20	142	2.98	0.15
121	1.10	0.21	143	1.37	0.43
122	1.22	0.42	144	0.82	0.24
123	0.44	0.18	145	1.78	0.24
124	1.14	0.34	146	0.40	0.42
125	0.98	0.14	147	0.30	0.54
126	1.66	0.02	148	1.70	0.48
127	2.32	0.42	149	2.92	−0.01
128	2.11	0.05	150	2.13	0.45
129	2.20	0.19	Average	2.37	0.12
130	0.75	0.33	Std Deviation	1.78	0.19

The scatter diagram of the correlation coefficient and difference for collapsed and survived buildings is showed in **Figure 5**. The collapsed buildings are shown by red triangles whereas the survived buildings by green circles. The average value for the collapsed buildings is shown by a black filled triangle, and that for the survived buildings by a black filled circle. The plus and minus standard deviations are shown by the error bar. From the figure, the correlation coefficient of the survived buildings is very high while the difference is close to zero, which indicates the change due the earthquake was small. On the other hand, the correlation coefficients of the collapsed buildings are low compared with those of the survived buildings, and their difference values are distributed widely.

In this study, we used these two indices to extract damaged buildings. In order to obtain the best threshold values for damage extraction, the cumulative distribution of the average values of the correlation coefficient within the layover area and that of the average value of the difference within the layover area are shown in **Figure 6 (a)** and **(b)**, respectively. In these plots, the cumulative probability of the plotting point i is $i/(n+1)$ with n indicating the number of samples.

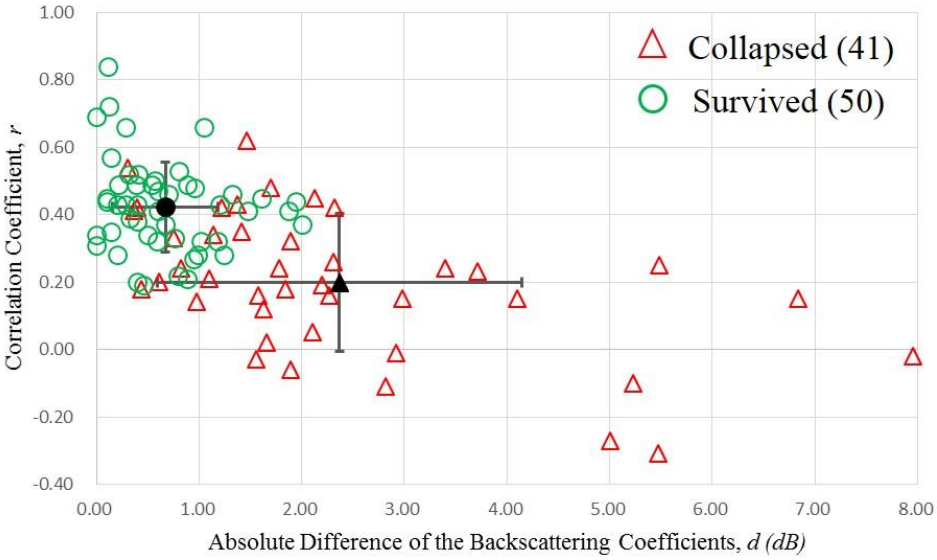

Figure 5. Scatter diagram of the correlation coefficient and backscattering difference for collapsed and survived buildings

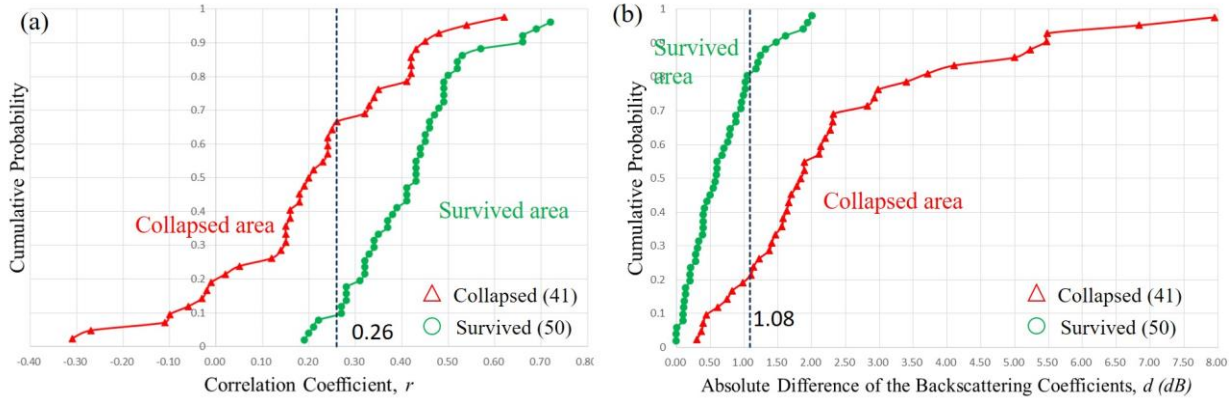

Figure 6. Cumulative probability of the **(a)** correlation coefficient and **(b)** difference value for the 41 collapsed and 50 survived buildings

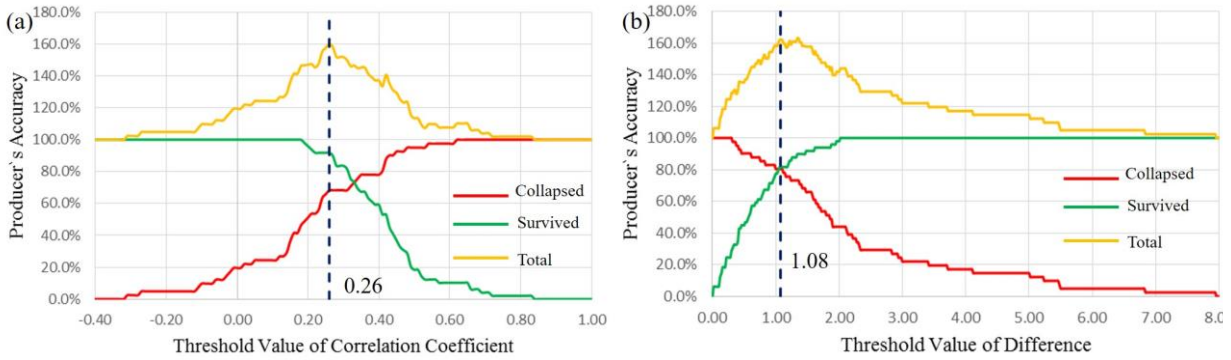

Figure 7. **(a)** Change of producer accuracy of collapsed (red line) and survived (green line) buildings and the sum of the both producer accuracies (yellow line) when the threshold of correlation coefficient moves from -0.4 to 1.0 continuously; and **(b)** those when the threshold of the difference moves from 0 dB to 8 dB.

Figure 7(a) shows the change of the producer accuracy for collapsed buildings (red line), survived buildings (green line), and the sum of the both producer accuracies (yellow line), when the threshold of the correlation coefficient moves from -0.4 to 1.0 continuously. From this figure, the largest sum of the producer accuracies was obtained for the threshold value of 0.26 for the correlation coefficient. **Figure 7(b)** shows the similar plot when the difference threshold moves from 0 dB to 8 dB. When the threshold of the difference was 1.33, the total producer accuracy became largest (165%) as shown in **Figure 7(b)**. However, the goal of this study is to extract the collapsed buildings, so we chose 1.08 as the threshold of the difference that is possible to extract more collapsed buildings, compared with the threshold value 1.33. Then the total producer accuracy for the threshold 1.08 was 164.2%, 0.8% lower compared to the result for the threshold 1.33. We plot this threshold in **Figure 6**. The left part of the threshold called "Collapsed area" whereas the right part of the threshold called "Survived area". On the other hand, **Figure 6(b)** shows the opposite of **Figure 6(a)**. Four survived buildings entered "Collapsed area" while 13 collapsed buildings were misclassified as shown in **Figure 6(a)**. **Figure 6(b)** shows 8 collapsed buildings entered "Survived area" while 9 of 50 survived buildings were misclassified.

The error matrix of the result based on the threshold values for the correlation coefficient and backscattering difference is shown in **Table 2**. According to this table, the producer's accuracy of the collapsed buildings is only 68.3% that is quite low compared to that for the survived buildings, which is 92.0%. On the other hand, the user's accuracy for collapsed buildings is quite high as 87.5% compared to the one for survived buildings, which is 78.0%. Thus, the overall accuracy based on the correlation coefficient is 81.3%. In this study, we selected 41 collapsed buildings and 50 survived buildings, which were the close population with high credibility. Many of previous studies used few collapsed buildings compared to survived buildings that made the overall accuracy quite high (Uprety et al., 2013 and Yamazaki et al., 2013). In order to remove the random coincidence rate, we calculated the kappa coefficient for the correlation coefficient, which is 0.615. This value means substantial agreement for the correlation coefficient in this study. **Table 2** show the producer's accuracy of the collapsed building is 80.5%, which is almost the same with the one for survived buildings (82.0%). While the user's accuracy of collapsed

Table 2. Error matrix classification of the result based on the thresholds of the correlation coefficient and absolute difference of the backscattering coefficient.

		Correlation coefficient				Difference			
		Reference Data				Reference Data			
		Collapsed	Survived	Total	UA	Collapsed	Survived	Total	UA
Image Interpretation	Collapsed	28	4	32	87.5%	33	9	42	78.6%
	Survived	13	46	59	78.0%	8	41	49	83.7%
	Total	41	50	91		41	50	91	
	PA	68.3%	92.0%			80.5%	82.0%		
	Overall Accuracy				81.3%	Overall Accuracy			81.3%
	Kappa Coefficient				0.615	Kappa Coefficient			0.624

building is 78.6% that is lower than the one for survived buildings (83.7%). Thus, the overall accuracy based on the difference threshold is 81.3%, the same to the result for the correlation coefficient. However, the kappa coefficient for the difference is 0.624, a bit higher than the result for the correlation coefficient.

In the near future, we are going to perform automatically extraction method in order to create rapid damage map after earthquake occurred. This method have many limitations such as we have to create rooftop of buildings, to know the height of each buildings in order to calculate length of the layover of each buildings, etc. so it will take quite much time to create these things. Thus in next study, we are going to create grid for the whole study area automatically in short time. We hope using this method rapid damage map can be created precisely and fast.

4. CONCLUSIONS

In this study, multi-temporal high-resolution TerraSAR-X images were used for damage inspection of the Kathmandu area, which was severely affected by the Mw 7.8 Gorkha, Nepal earthquake on 25 April 2015. The SAR images obtained before and after the earthquake were utilized for calculating the difference and correlation coefficient of the backscattering coefficient values within the layover and roof-print of an individual building. We chose 41 collapsed buildings and 50 survived buildings in the central part of Kathmandu using the pre- and post-event high resolution optical images, aerial video footages, and field survey photos as references. The affected areas were characterized by a low correlation coefficient and a high absolute difference. A threshold value of the correlation coefficient and difference was determined for training areas in the central Kathmandu. As a result, the overall accuracy of correlation coefficient was 81.3% with the kappa coefficient 0.613, whereas the overall accuracy for the difference was also 81.3 % with the kappa coefficient 0.624, which indicates high level of agreement.

We are going to create a rapid damage map by these threshold values in the target area in the near future. We hope this kind of damage maps can provide early stage information on the damage of built environments.

ACKNOWLEDGEMENT

The TerraSAR-X data are the property of the German Aerospace Center (DLR) and Inforterra GmbH and were made available by the PASCO Corporation through the joint research between PASCO Co. and Chiba University.

REFERENCES

Bahri, R., Liu, W., and Yamazaki, F., 2015. Damage assessment of buildings in Kathmandu due to the 2015 Nepal earthquake using TerraSAR-X imagery. Proc. 60th Spring Conference of the Remote Sensing Society of Japan, pp 15-18.

Brown, L.G., 1992. A survey of image registration techniques. ACM Computing Surveys, 24 (4).

Brunner D., Lemoine G. and Bruzzone L. 2010. Earthquake damage assessment of buildings using VHR optical and SAR imagery. IEEE Transactions on Geoscience and Remote Sensing, 48(5), pp 2403–2420.

Dell'Acqua, F., & Gamba, P. 2012. Remote sensing and earthquake damage assessment experiences, limits, and perspectives, Proceedings of the IEEE, 100, 2876–2890.

Ito, Y., Hosokawa, M., Lee, H., and Liu, J.G., 2000. Extraction of damaged regions using SAR data and neural networks. International Archives s of Photogrammetry and Remote Sensing 2000, XXXIII, pp.156–163

Lee, J.S., 1980. Digital image enhancement and noise filtering by use of local statistics. IEEE Transaction on Pattern Analysis and Machine Intelligence, 2(2), pp.165-168.

Liu, W., Yamazaki, F., Gokon, H., and Koshimura, S., 2013. Extraction of tsunami-flooded areas and damaged buildings in the 2011 Tohoku-Oki Earthquake from TerraSAR-X intensity images. Earthquake Spectra, 29(S1), S183-S200.

Matsuoka, M., and Yamazaki, F., 2004. Use of satellite SAR intensity imagery for detecting building areas damaged due to earthquakes. Earthquake Spectra 2004, 20(3), pp. 975-994.

Miura, H., Midorikawa, S., and Matsuoka, M., 2016. Building damage assessment using high-resolution satellite SAR images of the 2010 Haiti Earthquake. Earthquake Spectra, Vol 32, No. 1, pp 591-610.

PASCO Co., 2016. TerraSAR-X Basic Image Products. Retrieved February 15, 2016 from http://www.pasco.co.jp/eng/products/terrasarx/

Uprety, P., and Yamazaki, F., 2012. Detection of building damage in the 2010 Haiti earthquake using high-resolutin SAR intensity images. Journal of Japan Association for Earthquake Engineering, Vol. 12, No. 6, pp 21-35.

Uprety, P., and Yamazaki, F., Dell' Acqua, F., 2013. Damage detection using high-resolution SAR imagery in the 2009 L'Aquila, Italy, Earthquake. Earthquake Spectra, Vol. 29, No. 4, pp.1521-1535.

Yamazaki, Y., Iwasaki, Y., Liu, W., Nonaka, T., Sasagawa, T., 2013. Detection of damage to building side-walls in the 2011 Tohoku, Japan earthquake using high-resolution TerraSAR-X images, Proc. of SPIE Vol. 8892 889212-1.

Yonezawa, C., and Takeuchi, S. (2001). Decorrelation of SAR data by urban damages caused by the 1995 Hyogoken-Nanbu Earthquake, International Journal of Remote Sensing, 22:8, pp 1585–1600.